Time-Domain Harmonic Balance Method for Turbomachinery Aeroelasticity

Frédéric Sicot* and Adrien Gomar†
Centre Européen de Recherche et de Formation Avancée en Calcul Scientifique, 31057 Toulouse, France
Guillaume Dufour‡
Institut Supérieur de l'Aéronautique et de l'Espace (ISAE), Université de Toulouse, 31400 Toulouse, France
and
Alain Dugeai§
ONERA–The French Aerospace Lab, 92322 Châtillon, France

The present paper investigates a time-domain harmonic balance method as an alternative to classical time-marching schemes for stability studies of turbomachineries toward flutter. A weak-coupling approach is applied, which requires computing the fluid response to prescribed harmonic motions of the structure. The harmonic balance method, formulated in the arbitrary Lagrangian/Eulerian framework, is adapted to single-passage reduction using phase-lag boundary conditions expressed purely in the time domain. Validation against experimental data for the 11th standard configuration for aeroelasticity is performed, showing good agreement. Finally, an industrial test case is presented: a fan designed by Safran Snecma. The results show the good accuracy of the proposed harmonic balance method as well as significant reductions in computational time.

Nomenclature

B	=	number of blades
c	=	blade chord
d_m	=	harmonic balance source term coefficient
$\mathcal{D}$	=	mode diagonal matrix, $\mathcal{D}_{k,k}$ equals k
D_A, K_A, F_A	=	aerodynamic damping, stiffness, and force matrices
D_G, K_G	=	gyroscopic damping and centrifugal stiffness matrices
D_t	=	harmonic balance time-derivative operator
$\mathcal{E}$	=	discrete Fourier transform matrix
f, f_c	=	frequency, f equals $1/T$; reduced frequency, f_c equals $\pi c f/U$
k	=	mode number, $k \in [-N, N]$
$\mathcal{M}$	=	interblade phase angle modulation matrix, $\mathcal{M}_{k,k}$ equals $e^{ik\beta}$
M, D, K	=	modal mass, damping, and stiffness matrices
N	=	number of harmonics
n_d	=	nodal diameter
p	=	Laplace variable
q	=	generalized coordinates
R	=	residuals operator
$s(s_D)$	=	mesh (deformation) speed
t, T, t^*	=	time, time period, pseudotime
U	=	fluid velocity
V	=	cell volume
W	=	fluid conservative variables
X	=	mesh coordinates
(x, r, θ)	=	cylindrical coordinates
y^+	=	dimensionless wall distance
α	=	aerodynamic damping
β	=	interblade phase angle, β equals $2\pi n_d/B$
Φ	=	structure modal basis
ω	=	angular frequency, ω equals $2\pi/T$
$\dot{\bullet}$	=	time derivative of $\bullet$
$\hat{\bullet}_k$	=	kth Fourier coefficient
$\bullet_n$	=	nth time instant, t_n identical to $nT/(2N+1)$
$\bullet^*$	=	concatenation, $\bullet^*$ equals $(\bullet_0, \ldots, \bullet_{2N})^\top$

*Senior Researcher, CFD Team; frederic.sicot@cerfacs.fr.
†Ph.D. Student, CFD Team; adrien.gomar@cerfacs.fr.
‡Associate Professor, Département Aérodynamique, Energétique et Propulsion, 10 Avenue Edouard Belin; guillaume.dufour@isae.fr.
§Research Engineer, Aeroelasticity and Structural Dynamics Department; alain.dugeai@onera.fr.

I. Introduction

WITH the trend to reduce weight and increase stage loading of aeroengine components, flutter predictions have become a crucial part of turbomachinery design. On one hand, preliminary design methods [1] can be used early in the conception process with reasonable accuracy. On the other hand, direct aeroelastic simulations are the best way to predict flutter [2] but are still too expensive in terms of computational cost for routine design investigations. A practical method is the so-called weak-coupling approach in which a computational fluid dynamics solver is used to predict the aerodynamic response of blades vibrating in a periodic prescribed motion according to a given structural mode previously computed by a computational structural mechanics solver. A stability analysis can then be performed in the frequency domain.

A reference approach for the calculation of unsteady flows is the resolution of the unsteady Reynolds-averaged Navier–Stokes (URANS) equations with a classical time-marching scheme such as the dual time stepping (DTS) method [3]. Alternatively, efficient Fourier-based methods for periodic flows have undergone major developments [4]. The basic principle is to decompose the time-dependent flow variables into Fourier series to make a time-domain problem equivalent to a frequency-domain problem, in which the complex Fourier coefficients are the new unknowns. Two strategies have been proposed to obtain the solution. The first one is to directly solve for the Fourier coefficients, using a dedicated frequency-domain solver, as proposed by He and Ning [5,6], yielding the nonlinear harmonic method [7]. The second strategy is to cast the problem back to the time domain using the inverse Fourier transform,

as proposed by Hall et al. [8], Gopinath and Jameson [9], and Ekici et al. [10] with the harmonic balance (HB) method. The unsteady time-marching problem is thus transformed into a set of steady problems coupled by a spectral time-derivative operator. The main advantage of solving in the time domain is that it can be implemented in an existing classical Reynolds-averaged Navier–Stokes (RANS) solver, taking advantage of all classical convergence-accelerating techniques for steady-state problems. The HB method thus directly converges to the periodic state and avoids time-consuming unsteady transients. The present implementation was developed in the elsA [11] code by Sicot et al. [12] and extended to an arbitrary Lagrangian/Eulerian (ALE) formulation by Dufour et al. [13] to perform a weak fluid–structure coupling simulation for external flows. The HB method has been extensively applied and validated for external flows [14–17], considering both aerodynamics and aeroelasticity. However, when it comes to turbomachinery aeroelasticity, validation against experimental data remains an open issue [18–23].

Turbomachinery simulations are seldom performed on the whole circumference of the annulus due to the high computational cost. Cyclic periodicity is assumed, both for structure and fluid, which allows to solve for only one blade passage and thus drastically reduces the computational domain. In this case, the blades do not necessarily vibrate in phase, and an interblade phase angle (IBPA) can be prescribed according to a so-called nodal diameter. The phase-lag periodic condition (see [24] for the URANS approach) must then be applied on the azimuthal boundaries of the blade passage. However, it tends to increase the transient behavior needed by classical time-marching algorithms to reach the periodic state (see, for instance, [25]), which prompts for the use of an alternative method such as the HB technique. The first specific contribution of the present article is to apply the phase-lagged boundary conditions purely in the time domain (as described in [26] for rotor/stator interactions), as opposed to the mixed treatment in the Fourier space reported in the literature [8,27]. The advantage of this approach is that it is efficient, and easier to implement, because the phase-shifted flow solutions are computed analytically as a combination of all the computed snapshots, which are readily available in a time-domain harmonic approach.

The present study aims at validating the HB method for the prediction of aerodynamic loads on vibrating blades and at demonstrating its capability for a typical industrial application. First, the fluid/structure interaction in a weak-coupling approach is presented, with an emphasis on single-passage reduction. Second, the classical DTS technique and the HB method are presented and adapted to moving grids and single-passage reduction. Then, the 11th standard configuration [28] is investigated to validate the proposed approach. To the authors' knowledge, this is the first published article on the validation of HB results against aeroelastic experimental data in turbomachines. (Although since the present paper was submitted, the paper [29] was published.) Finally, because most contributions on the topic of HB simulations for turbomachinery aeroelasticity consider two-dimensional and/or inviscid test cases, a complex industrial fan designed by Snecma is considered. This application case includes a three-dimensional geometry with tip clearance and is treated with a RANS approach in order to demonstrate the robustness and the maturity of the harmonic balance method.

II. Fluid/Structure Interaction

A. Weak-Coupling Approach

The weak-coupling approach [2] is a one-way coupling from structure to fluid. First, a modal identification of the structure is carried out. Then, the fluid response to the harmonic prescribed motion of the structure modes is simulated, in which the harmonic motion of the geometry is ensured by a mesh deformation technique, based on a structural analogy method implementing linear elastic elements. Finally, knowing the unsteady pressure load, a stability study can be performed in the frequency domain.

B. Linear Modal Structure Model

1. Governing Equations

Once the modal basis Φ is identified, either by mean of a finite element model or an experimental identification, the equation of structure dynamics under aerodynamic load F_A reads

$$M\ddot{q} + D\dot{q} + Kq - \Phi^{\top} F_A(t) = 0, \qquad x = \Phi q \tag{1}$$

The weak-coupling approach assumes the linearity of the response of the fluid with respect to the displacement of the structure. Therefore, small displacements are assumed, and the so-called generalized aerodynamic forces are linearized, which adds aerodynamic stiffness K_A and damping D_A:

$$\Phi^{\top} F_A(t) = D_A \dot{q} + K_A q \tag{2}$$

To estimate the unsteady aerodynamic forces $F_A(t)$, a fluid simulation is run with a prescribed harmonic motion of the structure:

$$q(t) = \cos(\omega t) \tag{3}$$

A stability analysis is then performed in the frequency domain:

$$q = \hat{q} e^{pt} \Rightarrow (p^2 M + p(D - D_A) + (K - K_A))\hat{q} = 0 \tag{4}$$

where the Laplace variable p is of the form $p = i\omega(1 + i\alpha)$. Finally, considering only weakly damped or amplified modes (i.e., $|\alpha| \ll 1$), the damping of the fluid/structure coupled system reads $\alpha = -\Re e(p)/\Im m(p)$.

2. Single-Passage Reduction for Turbomachinery Computations

As the blade row is rotating, the stiffness of the blades is increased, and gyroscopic terms are added. Eq. (1) becomes

$$M\ddot{q} + (D + D_G)\dot{q} + (K + K_G)q - \Phi^{\top} F_A(t) = 0, \qquad x = \Phi q \tag{5}$$

where D_G is the skew-symmetric gyroscopic damping matrix and K_G is the gyroscopic matrix of deflection for inclusion of centrifugal elements for instance. The disk being flexible, the blades do not vibrate independently of each other. The cyclic symmetry leads to complex vibration modes, which can be seen as rotating waves traveling at an integer multiple n_d of the rotation speed [30]. n_d is called a nodal diameter. Opposite nodal diameters have the same vibration mode propagating in opposite directions. Therefore, their respective modes are complex conjugate.

C. Nonlinear Aerodynamic Model

1. Governing Equations

The URANS equations are written in finite-volume semidiscrete form with ALE formulation as

$$\frac{\partial (VW)}{\partial t} + R(W, s) = 0 \tag{6}$$

W is the vector of conservative variables complemented with an arbitrary number of turbulent variables as within the RANS framework. The residuals $R(W, s)$ result from the spatial discretization of the convective and viscous fluxes in a mesh moving at speed s, the sum of the entrainment velocity and the deformation velocity s_D. Detailed formulation of the governing equations can be found in [13] for instance.

2. Single-Passage Reduction

To reduce the computational domain, Cinnella et al. [31] considered an annular sector of 360 deg $\cdot\, z$/IBPA of the annulus to have no lag at the azimuthal boundaries, where z is the minimum integer that leads to an integer number of blade passages. As a result, the size of the domain changes when considering different IBPAs,

up to the full annulus (for $n_d = 1$, for instance), which is not computationally efficient.

A more general approach is the phase-lag periodic condition [24], which allows to solve only one blade passage per row if no mistuning is involved, reducing dramatically the computational domain. It states that the flow in a blade passage at time t is the flow at the next passage but at another time $t + \beta/\omega$. This time lag corresponds to the phase of a rotating wave, i.e., an IBPA, depending on the nodal diameter: $\beta = 2\pi n_d/B$. As a property of the Fourier transform, the spectrum of the flow is then equal to the spectrum of the neighbor blade passage modulated by a complex exponential depending on the IBPA:

$$W\left(x, r, \theta + \frac{2\pi}{B}, t\right) = W\left(x, r, \theta, t + \frac{\beta}{\omega}\right) \tag{7}$$

is equivalent to

$$\hat{W}_k\left(x, r, \theta + \frac{2\pi}{B}\right) = \hat{W}_k(x, r, \theta)e^{ik\beta}, \quad \forall\ k \in \mathbb{Z} \tag{8}$$

The IBPA is associated to one frequency: the vibration frequency. This phase-lag method cannot take into account another IBPA, such as the one associated to the blade passing frequency of a neighbor row. As a consequence, the single-passage reduction is limited to an isolated row.

III. Time-Integration Schemes

A. Dual Time Stepping Method

The DTS method [3] is a second-order implicit time-marching scheme. A pseudotime t^* derivative is added to Eq. (6) in order to solve the induced nonlinear system at each time step:

$$V\frac{\partial W}{\partial t^*} + \frac{\partial (VW)}{\partial t} + R(W, s) = 0 \tag{9}$$

The inner iterations are equivalent to solve a steady problem, which cancels out the pseudotime derivative, and Eq. (6) is retrieved. The inner steady problem can benefit from convergence-acceleration techniques such as the multigrid technique [32] and local time stepping. One needs to find a tradeoff between the physical time step and the number of subiterations (i.e., the convergence of the inner loop), but the DTS method usually allows higher time steps compared to explicit schemes and thus reduces the computational cost.

The harmonic motion of the geometry is ensured by a mesh deformation technique, based on a structural analogy method implementing linear elastic elements. The deformation speed s_D is estimated thanks to a first-order finite-difference scheme between the mesh points at previous and current instants: $s_D(t_n) = (X_n - X_{n-1})/\Delta t$.

The phase-lag periodic condition is achieved thanks to a sliding Fourier decomposition as inspired by the shape correction method presented by He [33]. A phase-lag computation is usually initialized by a steady-state simulation with azimuthal rotation periodicity. Therefore, it requires more simulated time periods to trigger the phase lag and reach the periodic state than a regular rotation-periodicity simulation (e.g., a periodic sector as in [31] or when all blades vibrate in phase). The available literature [2,25] suggests that the simulation time needed to reach the periodic state is three times more important with phase-lag periodicity that with rotation periodicity. The DTS computation, if sufficiently sampled, is considered as the reference unsteady solution.

B. Harmonic Balance Method

1. Fourier-Based Time-Derivative Operator

If both the flow variables W and cell volume V are periodic in time with period $T = 2\pi/\omega$, so are the residuals $R(W, s)$, and the Fourier series of Eq. (6) reads

$$\sum_{k=-\infty}^{\infty} (ik\omega\widehat{VW}_k + \widehat{R}_k)\exp(ik\omega t) = 0 \tag{10}$$

The complex exponential family forming an orthogonal basis, the only way for Eq. (10) to be true is that the weight of every mode k is zero. An infinite number of steady equations are obtained in the frequency domain:

$$ik\omega\widehat{VW}_k + \widehat{R}_k = 0, \quad \forall\ k \in \mathbb{Z} \tag{11}$$

McMullen et al. [34] solved a subset of these equations up to mode N, $-N \le k \le N$, yielding the nonlinear frequency domain method. As the present HB method has to be implemented in the elsA code [11], which is a time-domain solver, these equations cannot be easily solved. The harmonic balance method [8] and the time spectral method [9] use an inverse discrete Fourier transform (IDFT) to cast back this subset of $2N + 1$ equations into the time domain. The IDFT induces linear relations between the Fourier's coefficients $\hat{W}_k$ and a uniform sampling of W within the period. Finally, the following matrix formulation is retrieved:

$$i\omega\mathcal{E}^{-1}\mathcal{D}\mathcal{E}(VW)^* + R^* = 0 \tag{12}$$

where $(VW)^*$ is a vector of a uniform sampling of the flow variables

$$W^* = [V_0W_0, \ldots, V_nW_n, \ldots, V_{2N}W_{2N}],$$
$$W_n = W\left(\frac{2\pi}{\omega}\frac{n}{2N+1}\right) \tag{13}$$

$\mathcal{E}$ is the discrete Fourier transform matrix:

$$\mathcal{E}_{n,k} = \frac{1}{2N+1}\exp(-i\omega_k t_n) = \frac{1}{2N+1}\exp\left(-2i\pi k\frac{n}{2N+1}\right) \tag{14}$$

and $D_{k,k} = k, k \in [-N, N]$. Gopinath and Jameson [9] provide an analytical derivation of the source term $i\omega\mathcal{E}^{-1}\mathcal{D}\mathcal{E}$ appearing in Eq. (12). This leads to a time discretization with a new time operator D_t as follows:

$$R(W_n, s_n) + D_t(V_nW_n) = 0, \qquad 0 \le n < 2N + 1 \tag{15}$$

These steady equations correspond to $2N + 1$ instants t_n evenly spaced within the period, such that $t_n = nT/(2N + 1)$. The new time operator connects all the time levels and is expressed analytically by

$$D_t((VW)^*) = i\omega\mathcal{E}^{-1}\mathcal{D}\mathcal{E}(VW)^* \Leftrightarrow D_t(V_nW_n) = \sum_{m=-N}^{N} d_m V_{n+m}W_{n+m} \tag{16}$$

with

$$d_m = \frac{\pi}{T}\frac{(-1)^{m+1}}{\sin(\pi m/2N+1)} \quad \text{if } m \neq 0 \quad \text{and} \quad d_0 = 0 \tag{17}$$

A pseudotime derivative $V_n\partial W_n/\partial t_n^*$ is added to Eq. (15) in order to time march these equations to the steady-state solutions of all the instants. The term $D_t(V_nW_n)$ appears as a source term that represents a high-order formulation of the initial time derivative in Eq. (6). Figure 1 shows the different states of the HB instants during the iteration process. Usually, all instants are initialized by the same initial condition (Fig. 1a). Then, at each pseudotime iteration, the HB time derivative D_t [Eq. (16)] is added as a source term. It is different from one instant to another because the deformed meshes are different and thus allow the instants to differentiate (Fig. 1b). In the end, once the steady convergence is reached, all the instants have converged toward the periodic flow (Fig. 1c).

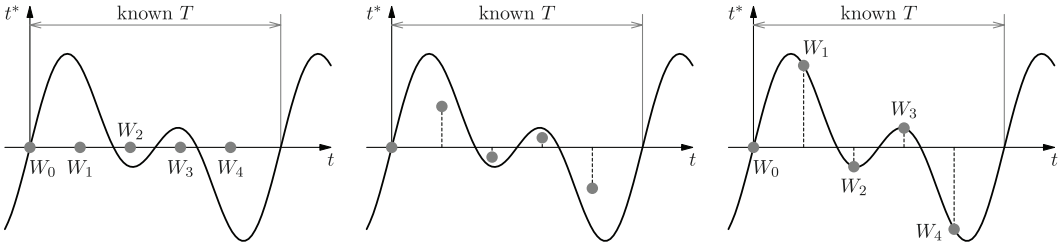

a) Initial condition **b) Intermediate state** **c) Final state**

Fig. 1 HB method iteration chart.

The pseudotime marching takes advantage of the same accelerating methods used in the inner loops of the DTS method. The implicit scheme is carried out by the Block-Jacobi Successive-over-relaxation implicit algorithm [12] developed to improve robustness.

2. Adaptation to the Arbitrary Lagrangian/Eulerian Formulation

The deformation speed s_D is estimated by applying the HB time-derivative operator to the mesh points at all instants: $s_D^* = D_t(X^*)$. This decomposition is exact when the deformation of the mesh has less harmonics than those solved in the HB computation [13]. In the present case, the mesh deformation follows a purely single-frequency law [see Eq. (3)]; therefore, all the HB computations will correctly estimate the mesh deformation speed regardless of their harmonic content.

3. Adaptation to Turbomachinery Single-Passage Reduction

The phase-lag periodic condition can be derived by applying an IDFT on the phase-shifted harmonics $\hat{W}_k e^{ik\beta}$ of Eq. (8). A linear combination of all the time instants is obtained:

$$W^*\left(\theta + \phi\frac{2\pi}{B}\right) = \mathcal{E}^{-1}\mathcal{M}\mathcal{E}W^*(\theta), \qquad \phi = \pm 1 \tag{18}$$

where $\mathcal{M}$ is a diagonal matrix equal to the IBPA modulation $\mathcal{M}_{k,k} = e^{ik\beta}$. It can be derived analytically in the same way as the source term Eqs. (16) and (17):

$$W\left(x, r, \theta + \phi\frac{2\pi}{B}, t_n\right) = \sum_{m=-N}^{N} b_m W(x, r, \theta, t_{n+m}) \tag{19}$$

with

$$b_m = \frac{1}{2N+1}\left(1 + 2\sum_{k=1}^{N}\cos\left[k\left(2\pi\frac{m}{2N+1} - \phi\beta\right)\right]\right), \quad \phi = \pm 1 \tag{20}$$

As the HB method solves and stores simultaneously a uniform sampling of the time period, it could be considered similar to Erdos' direct store method. Actually, the method used here is closer to the shape correction [33], in a sense that the lag is computed thanks to Fourier series.

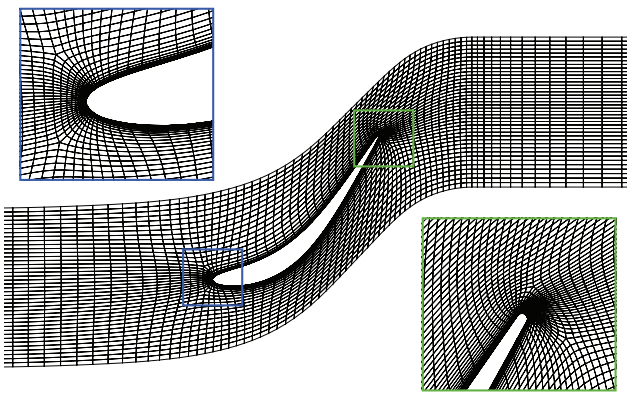

Fig. 2 STCF 11 mesh.

IV. Numerical Applications

For external-flow aeroelasticity, the HB approach has been thoroughly validated [9,12,13,16], mostly for the AGARD test cases of Davis [35]. However, experimental data for turbomachinery aeroelasticity are more scarce; the standard aeroelastic configurations experiments of Fransson et al. [28] are the reference in this respect and have been widely used to validate different numerical approaches [31,36–39]. However, this is the first time these results are used to validate HB simulations. The presented applications are in increasing complexity. The first test case is a turbine stator Standard Configuration (STCF 11), for which experimental results are available at both subsonic and transonic conditions. The second test case is an industrial fan configuration, proving the robustness of the method for industrial requirements.

A. 11th Standard Configuration

The 11th standard configuration is a turbine stator composed of 20 blades and tested at École Polytechnique Fédérale-Lausanne in the late 1990s by Fransson et al. [28]. The experimental results have been found to be highly reproducible and therefore suitable for code validation [28].

The geometry profile and the results are available over the internet[¶]. To allow local validation of the steady flow, the isentropic Mach number is given at the blade wall.

The blades oscillate harmonically in the first bending mode in an annular test rig at a reduced frequency of $f_c = \pi cf/U_{\text{outlet,exp}} = 0.2134$ for the subsonic case and 0.1549 for the transonic case. Aeroelastic results are available, such as the first harmonic of the unsteady pressure coefficient at blade walls (amplitude and phase), for several nodal diameters. The integrated results, such as the damping, strongly vary under small changes in the local distribution. It is therefore recommended to look at the local distributions.

The blade passage is meshed using an O4H topology (Fig. 2). The number of grid points along the blade chord axis is 160, and the computed y^+ at the walls is $\mathcal{O}(1)$. The blade has the same profile along the spanwise direction and no twist. Therefore, a 2.5-dimensional mesh is used with five points in the radial direction, with a spanwise extent representing 1% of the chord.

The boundary conditions used for this case include 1) an injection condition for the inlet (with a relative flow angle set to the experimental value), 2) a constant static pressure condition for the outlet, 3) an adiabatic no-slip condition on blade walls, and 4) periodic or phase-lagged conditions for azimuthal boundaries depending on the prescribed IBPA. Turbulence is modeled using the one-equation model of Spalart–Allmaras [40]. The third-order upwind Roe scheme [41] is used to compute the convective fluxes. The maximum Courant–Friedrichs–Lewy condition number is set to 20 for the steady computations, the inner loop of the DTS scheme, and the HB simulations. For the DTS scheme, convergence in time discretization is obtained after 20 periods using 128 instants per

[¶]Data available online at http://www.energy.kth.se/proj/projects/Markus%20Joecker/STCF/STCF11/stcf11.htm [retrieved 7 August 2013].

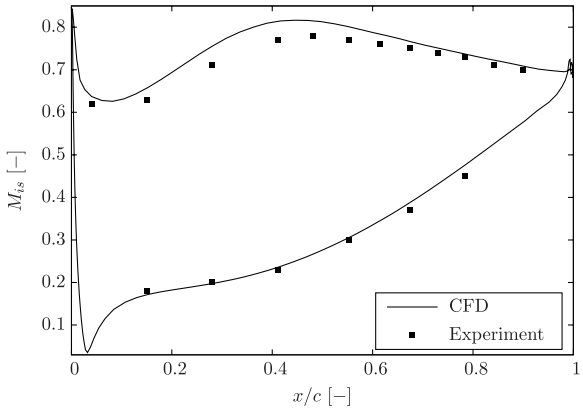

Fig. 3 Steady results of the isentropic Mach number at blade walls, subsonic case.

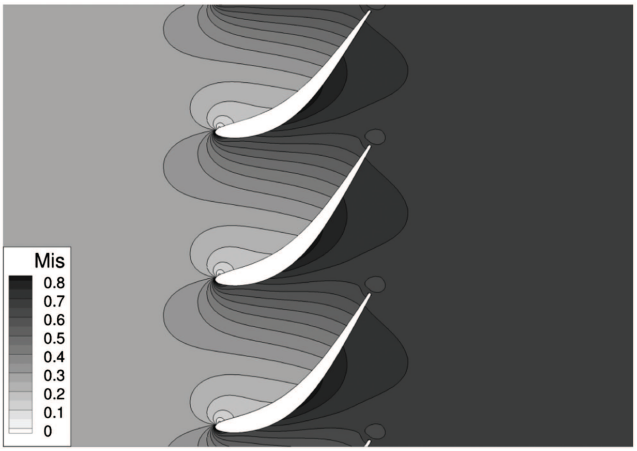

Fig. 4 Steady isentropic Mach number contours, subsonic case.

period. Iterative convergence for the inner loop is considered achieved when the normalized residuals drop by 5×10^{-2} (within a maximum of 50 subiterations).

1. Subsonic Case

The measured inlet Mach number is 0.31 and the isentropic outlet Mach number is 0.69. Steady results for the isentropic Mach number at blade walls are compared to the experimental data in Fig. 3. For this flow regime, the flow remains subsonic. On the pressure side, the flow accelerates all the way to the trailing edge of the blade. On the suction side, the flow accelerates until a maximum speed at ≈40% of the chord and then decelerates (Fig. 4). The agreement with the experimental data is fair. However, an overprediction of the isentropic Mach number is observed on the suction side. This discrepancy is also reported in the literature (see [28], for instance).

The aeroelastic experimental data are compared to the present results obtained with both the DTS and the HB approaches. To explore the range of nodal diameters with the HB method, an incremental approach is used in which each nodal diameter simulation is used to initialize the next one. Considering the opposite phase vibration case (the 10th nodal diameter), the amplitude and the phase of the pressure coefficient are presented in Fig. 5. With only one harmonic (i.e., three instants), the HB results are superimposed on the DTS ones. Moreover, the numerical results are in fair agreement with

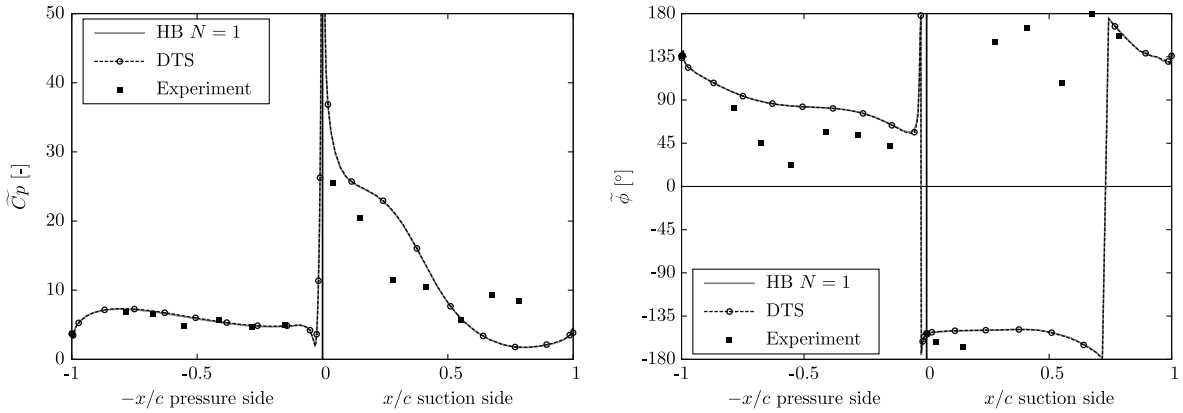

a) Amplitude part **b) Phase part**

Fig. 5 Wall pressure harmonic analysis for an opposite phase vibration, subsonic case.

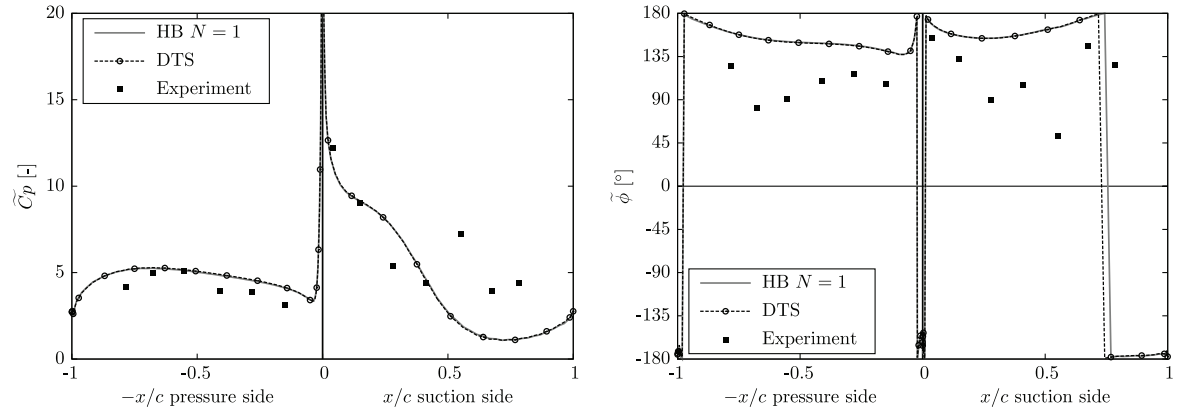

a) Amplitude part **b) Phase part**

Fig. 6 Wall pressure harmonic analysis for $n_d = -2$, subsonic case.

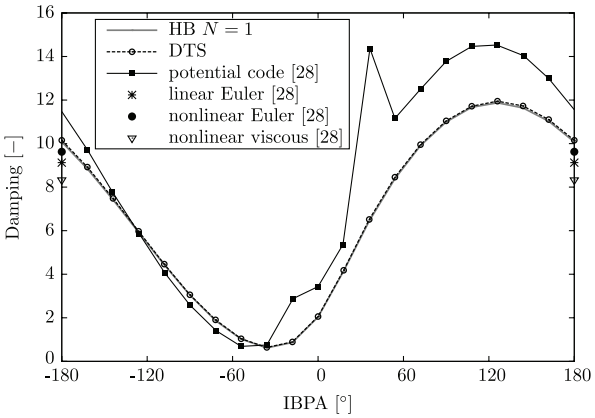

Fig. 7 Aerodynamic damping coefficient versus IBPA, subsonic case.

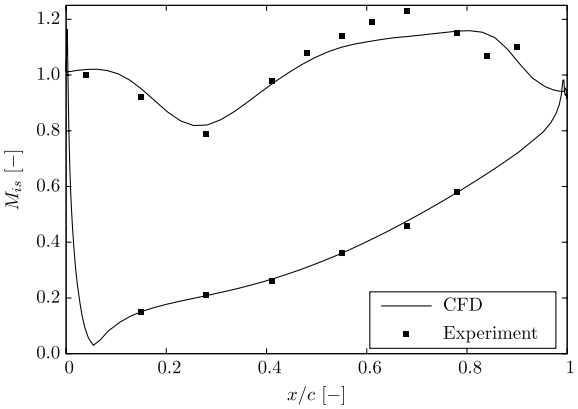

Fig. 8 Steady results of the isentropic Mach number at blade wall, transonic case.

the experimental data for the amplitude. However, for the phase, the sign change on the suction side is predicted at about 60% of the chord, whereas the experimental location is about 25%.

The results for the nodal diameter −2 are shown in Fig. 6. The HB and DTS data are superimposed and are in fair agreement with the experiments. The amplitude levels are well captured, and the phase prediction is slightly improved over the opposite phase case.

The damping obtained from the previous calculations is depicted in Fig. 7. Also plotted are the results from Fransson et al. [28], obtained with both potential, linear Euler, nonlinear Euler, and nonlinear viscous codes. The results for all IBPAs are given for the potential code, but only $\beta = 180$ deg is provided for the other codes [28]. These are the only damping results for the subsonic case known by the authors. Because the local variations are superimposed for the

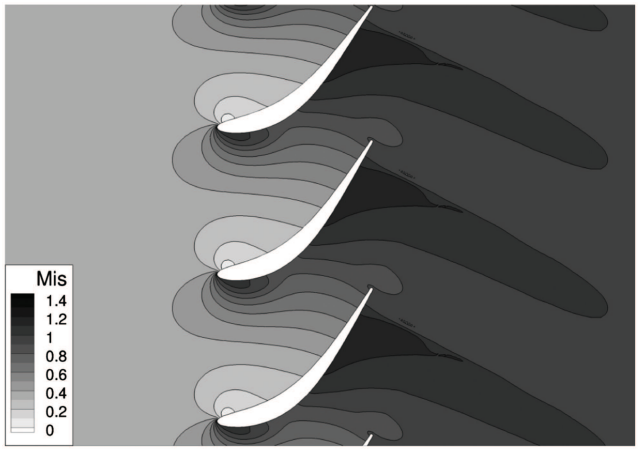

Fig. 9 Steady isentropic Mach number contours, transonic case.

DTS and the HB approaches, so are the damping. The present results show similar trends and levels to those of Fransson et al.

2. Transonic Condition

The outlet isentropic Mach number is 0.99 for an inlet Mach number of 0.4. This case, for which experimental uncertainties are available, has been largely addressed in the literature (see, for instance, [31,36–38]). This test case is challenging in terms of nonlinearities as a separation bubble and a shock are present.

Steady results of the isentropic Mach number are shown in Fig. 8. For this flow regime, a small separation bubble develops on the suction side at the leading edge (cf. Fig. 9). The flow then accelerates, followed by a passage shock. The experimental data suggest that the shock appears sooner on the suction side than in the computations; all the results reported in the literature exhibit similar discrepancies (see [28,31,36–38]). Otherwise, the present results are in fair agreement with experimental data.

The aeroelastic experimental data are compared to the present results obtained with both the DTS and the HB approaches. Considering the opposite phase vibration case (the 10th nodal diameter), the amplitude and the phase of the pressure coefficient are presented in Fig. 10. Also plotted are the results of Cinnella et al. [31], computed with a nonlinear viscous approach using the Spalart–Allmaras turbulence model. The present HB and the DTS results are superimposed, which indicates that the one harmonic HB solution is able to reproduce the unsteady nonlinear effects without increasing the number of harmonics. This observation is only valid near the wall, before the harmonics are created naturally by the flow, due to the nonlinear effects. The results are in good agreement with the experimental data and display the same trends as that of Cinnella et al. A slight discrepancy can be observed within the shock region, in which the amplitude and the phase phenomena are predicted further

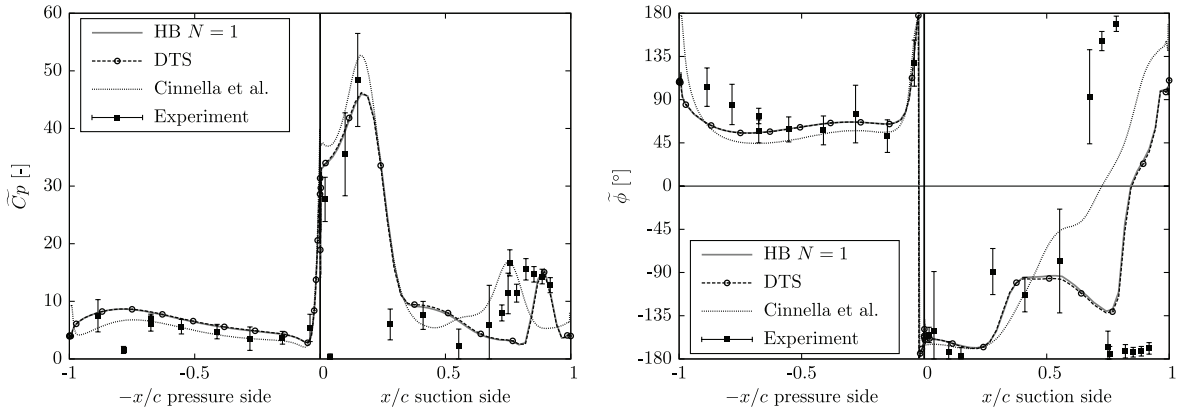

a) Amplitude part **b) Phase part**

Fig. 10 Wall pressure harmonic analysis for an opposite phase vibration, transonic case.

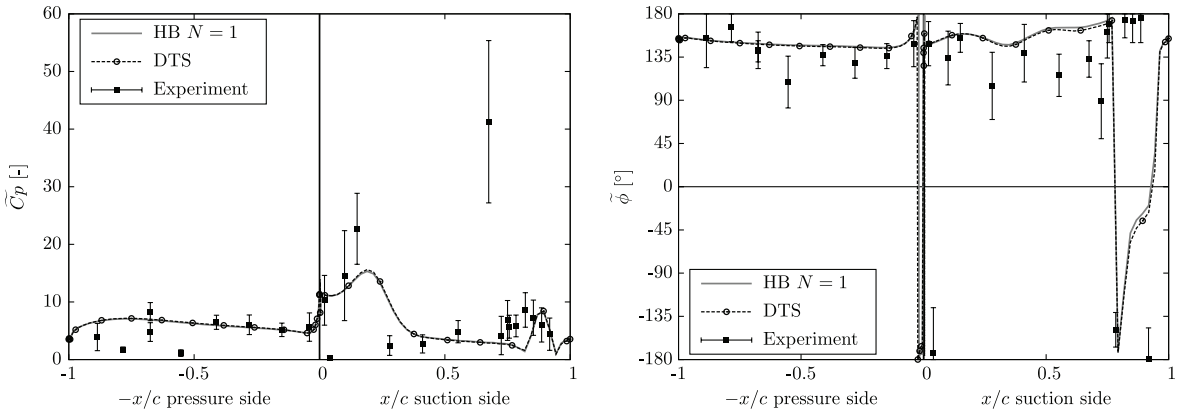

a) Amplitude part **b) Phase part**

Fig. 11 Wall pressure harmonic analysis for $n_d = -2$, transonic case.

than the experiments indicate. This can be attributed to the poor prediction of the shock position and hence the poor prediction of its interaction with the motion of the blade.

The results for the nodal diameter −2 are also shown in Fig. 11. Again, the HB results are superimposed on the DTS ones. Moreover, these are in good agreement with the experiments, considering the uncertainties of the experimental data.

The damping is shown in Fig. 12 for the transonic case. Also plotted are the results from Fransson et al. (potential code) [28] and from Cinnella et al. (RANS) [31]. The scattering is much more severe than for the subsonic case. The trends obtained with the RANS approaches are similar. However, the discrepancies between the two RANS codes are significant in terms of levels. Recently, Vogt and Fransson [42] reported similar discrepancies for damping predictions of subsonic and transonic cascades, showing that the damping can be significantly affected by small local changes in the amplitude and/or the phase. In terms of computational efficiency, the HB method is seven times faster than the DTS for all the IBPAs.

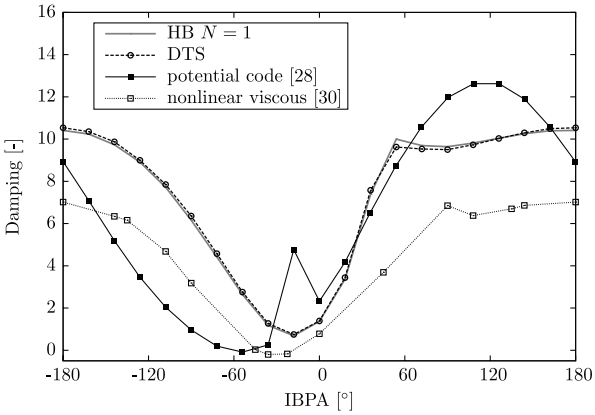

Fig. 12 Aerodynamic damping coefficient versus IBPA, transonic case.

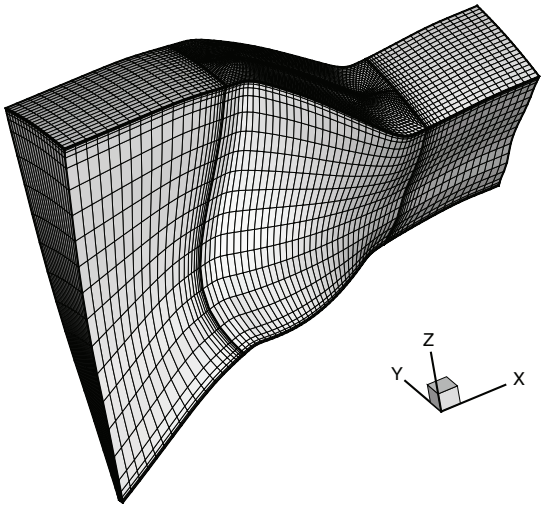

Fig. 13 Fan mesh (for a better readability, the mesh is coarsened by a factor 2 in every direction).

B. Safran Snecma Fan

The third test case is a transonic fan designed by Safran Snecma. Because of confidentiality reasons, the authors cannot show all nodal

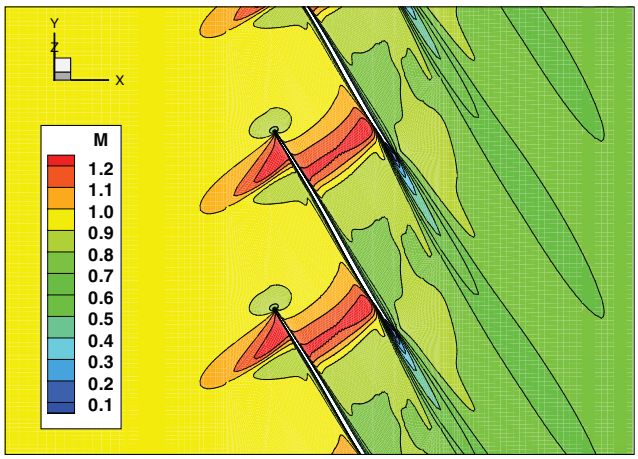

Fig. 14 Instantaneous Mach contours (95% span).

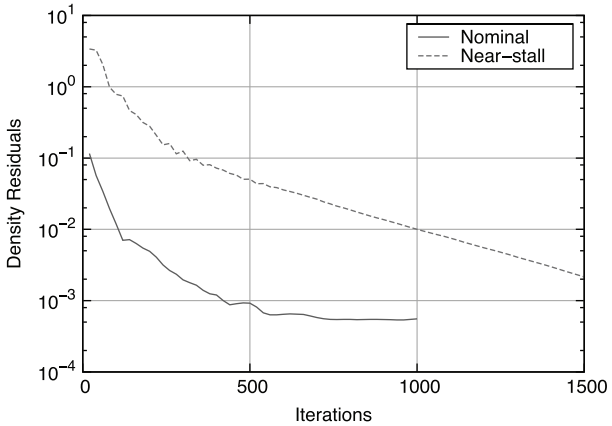

Fig. 15 HB residuals convergence (three instants, $n_d = 1$).

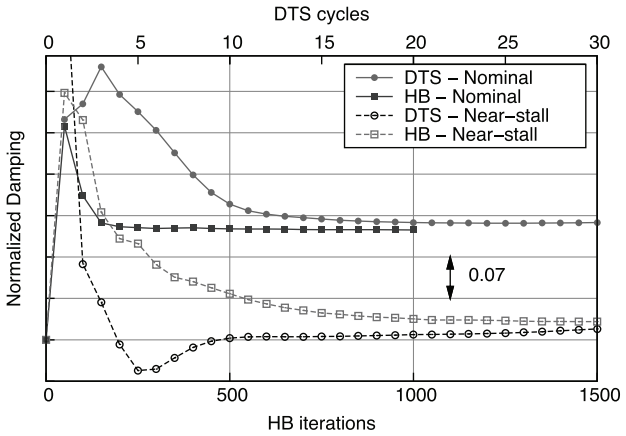

Fig. 16 Comparison of damping convergence ($n_d = 1$).

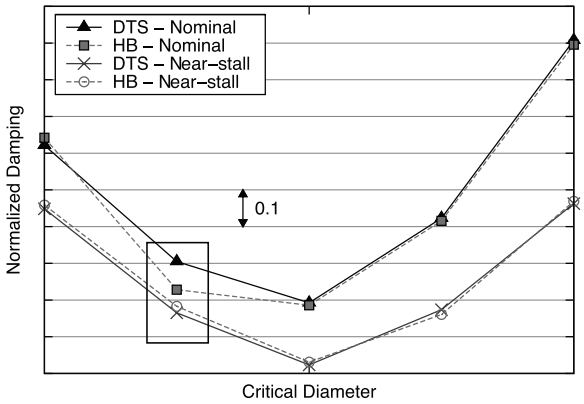

Fig. 17 Normalized fan aerodynamic damping.

diameters and have to normalize the aerodynamic damping. The Reynolds number based on tip speed is about 14×10^6. The motion simulated is the first bending mode, at a reduced frequency $f_c = \pi c f / U = 0.26$, for an amplitude small enough to be within the linear domain. The low-Reynolds mesh is shown Fig. 13 and comprises about 800,000 cells. The instantaneous Mach contours (Fig. 14) present strong shocks that spread over the blade passage.

The numerical parameters stem from industrial best practices. Turbulence is modeled by the one-equation model of Spalart–Allmaras [40]. The spatial scheme of Jameson et al. [43] is used. The DTS computation is performed on 30 periods with 64 instants per period. The subiterations are considered as converged when the normalized residual have dropped by 5×10^{-2} with a maximum of 20 subiterations. The time step and the number of periods simulated to reach the periodic state have been verified to yield a time-converged solution. All the steady problems (HB and DTS subiterations) benefit from local time stepping and a multigrid cycle with one coarse level.

Two operating points are studied: the nominal point and a near-stall point. The convergence of the HB method with three instants is shown in Fig. 15. Although the nominal point requires less than 1000 iterations to converge, the near-stall point is still converging after 1500 iterations. This was expected as near-stall operating point are usually numerically "stiffer." Nevertheless, the normalized damping (Fig. 16) converges faster than the residuals as about 300 iterations are sufficient for the nominal case and 1000 for the near-stall case. The results match the DTS damping quite well.

The aerodynamic damping is given in Fig. 17 for some diameters around the critical diameter (i.e., the diameter with the lowest damping). All diameters give a positive damping, for both operating

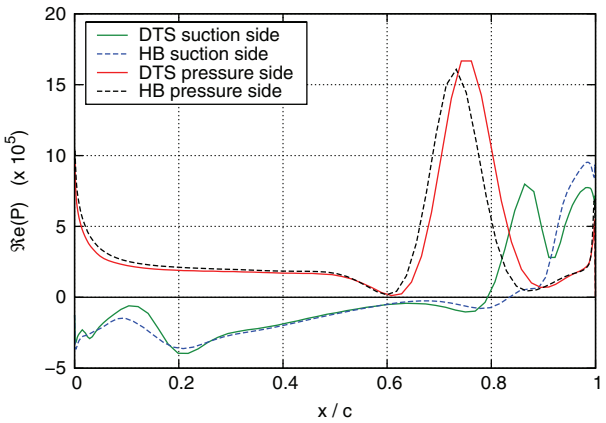

Nominal point – Real part

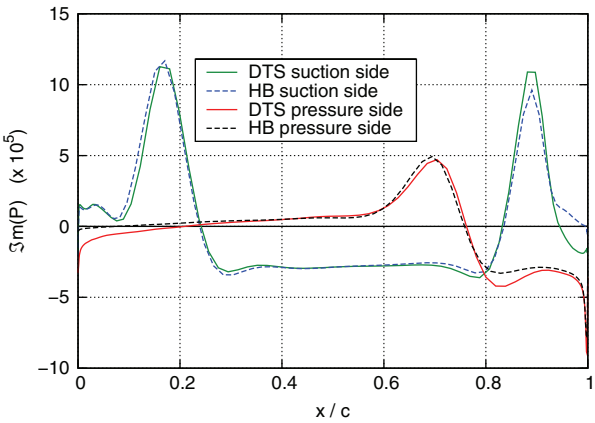

Nominal point – Imaginary part

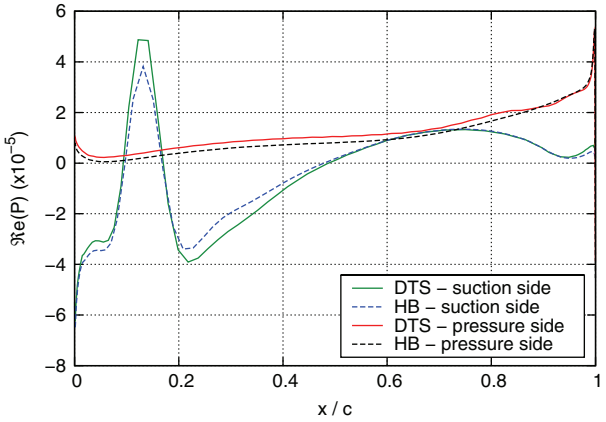

Near-stall point – Real part

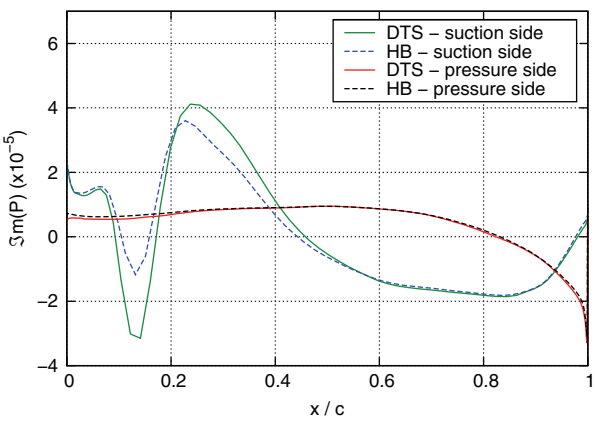

Near-stall point – Imaginary part

Fig. 18 Wall pressure harmonic analysis in the worst case (90% span).

points, which clears this fan for flutter problems. The critical diameter is the same for both operating points and both time-integration schemes. The HB results are superimposed on the reference computation in the near stall case, which is surprising as it is numerically stiffer due to detached flow regions in which the flow spectrum is expected to be richer than the HB method can capture. Figure 18 gives the harmonic analysis of the wall pressure at 90% of the blade span for the diameter below the critical one, in which the highest gap between DTS and HB methods is observed (in the rectangle on Fig. 17). Both time-integration schemes give similar results. Concerning the nominal point, the highest discrepancies appear on the real part of the first harmonic in the last 20% of the chord on the suction side. The HB method also tends to underestimate the amplitude of unsteadiness in the first 40% of the chord of the suction side in the near-stall case.

The HB gains in computational cost compared to the DTS method range from 3 to 10 times faster. It is found that the gain of the HB approach over the DTS method increases with the value of the IBPA, mostly due to the fact that the HB method takes full advantage of the initialization with the previous IBPA computation, without any loss in convergence rate, whereas the DTS computations converge more slowly as the blades tend to vibrate in opposite phase.

V. Conclusions

The HB approach for aeroelastic damping calculation, derived for periodic problems in which the period is known a priori, has been presented. The phase-lagged boundary conditions are then purely derived in the time domain, which is expected to be more computationally efficient and easier to implement. Finally, the proposed method has been validated on the 11th standard configuration and applied to an industrial case. The results show that the HB approach provides local and global results close to the reference DTS scheme with only three instants (one harmonic) in the time period. At the cost of a memory increase (roughly equal to the number of instants used in the HB simulations), the computational saving is about a factor 3 to 10, depending on the case considered, the operating point, and the value of the IBPA. For the 11th standard configuration, the results are in good agreement with the experimental data and with the results found in the literature. For the fan case considered in the present study, the critical damping is well predicted at the nominal point. In practice, the HB method is a good candidate for fast preliminary design investigations, which could be complemented by more advanced studies.

Acknowledgments

The present Harmonic Balance formulation was developed thanks to the support of the Direction des Programmes Aéronautiques Civils (French Civil Aviation Agency) and of the Aerospace Valley (world competitiveness cluster Midi-Pyrénées and Aquitaine). The authors would also like to thank Snecma from the Safran group for their kind permission to publish this study.

References

[1] Kielb, R., Barter, J., Chernycheva, O., and Fransson, T. H., "Flutter of Low Pressure Turbine Blades with Cyclic Symmetric Modes: A Preliminary Design Method," *Journal of Turbomachinery*, Vol. 126, No. 2, 2004, pp. 306–309. doi:10.1115/1.1650380

[2] Rougeault-Sens, A.-S., and Dugeai, A., "Numerical Unsteady Aerodynamics for Turbomachinery Aeroelasticity," *Unsteady Aerodynamics, Aeroacoustics and Aeroelasticity of Turbomachines*, edited by Hall, K. C., Kielb, R. E., and Thomas, J. P., Springer–Verlag, Dordrecht, The Netherlands, 2006, pp. 423–436.

[3] Jameson, A., "Time Dependent Calculations Using Multigrid, with Applications to Unsteady Flows Past Airfoils and Wings," *10th Computational Fluid Dynamics Conference*, AIAA Paper 1991-1596, June 1991.

[4] He, L., "Fourier Methods for Turbomachinery Applications," *Progress in Aerospace Sciences*, Vol. 46, No. 8, 2010, pp. 329–341. doi:10.1016/j.paerosci.2010.04.001

[5] He, L., and Ning, W., "Efficient Approach for Analysis of Unsteady Viscous Flows in Turbomachines," *AIAA Journal*, Vol. 36, No. 11, 1998, pp. 2005–2012. doi:10.2514/2.328

[6] Ning, W., and He, L., "Computation of Unsteady Flows Around Oscillating Blades Using Linear and Nonlinear Harmonic Euler Methods," *Journal of Turbomachinery*, Vol. 120, No. 3, 1998, pp. 508–514. doi:10.1115/1.2841747

[7] Vilmin, S., Hirsch, C., Lorrain, E., and Swoboda, M., "Unsteady Flow Modeling Across the Rotor/Stator Interface Using the Nonlinear Harmonic Method," *ASME Turbo Expo*, ASME Paper GT-2006-90210, May 2006.

[8] Hall, K. C., Thomas, J. P., and Clark, W. S., "Computation of Unsteady Nonlinear Flows in Cascades Using a Harmonic Balance Technique," *AIAA Journal*, Vol. 40, No. 5, May 2002, pp. 879–886. doi:10.2514/3.15137

[9] Gopinath, A., and Jameson, A., "Time Spectral Method for Periodic Unsteady Computations over Two- and Three- Dimensional Bodies,"*43rd AIAA Aerospace Sciences Meeting and Exhibit*, AIAA Paper 2005-1220, Jan. 2005.

[10] Ekici, K., Hall, K. C., and Dowell, E. H., "Computationally Fast Harmonic Balance Methods for Unsteady Aerodynamic Predictions of Helicopter Rotors," *Journal of Computational Physics*, Vol. 227, No. 12, 2008, pp. 6206–6225. doi:10.1016/j.jcp.2008.02.028

[11] Cambier, L., Heib, S., and Plot, S., "The Onera elsA CFD Software: Input from Research and Feedback from Industry," *28th Congress of the International Council of the Aeronautical Sciences*, International Council of the Aeronautical Sciences Paper 2012-2.1.1, Sept. 2012.

[12] Sicot, F., Puigt, G., and Montagnac, M., "Block-Jacobi Implicit Algorithms for the Time Spectral Method," *AIAA Journal*, Vol. 46, No. 12, 2008, pp. 3080–3089. doi:10.2514/1.36792

[13] Dufour, G., Sicot, F., Puigt, G., Liauzun, C., and Dugeai, A, "Contrasting the Harmonic Balance and Linearized Methods for Oscillating-Flap Simulations," *AIAA Journal*, Vol. 48, No. 4, 2010, pp. 788–797. doi:10.2514/1.43401

[14] Liu, L., Dowell, E. H., and Thomas, J. P., "A High Dimensional Harmonic Balance Approach for an Aeroelastic Airfoil with Cubic Restoring Forces," *Journal of Fluids and Structures*, Vol. 23, No. 3, 2007, pp. 351–363. doi:10.1016/j.jfluidstructs.2006.09.005

[15] Dimitriadis, G., "Continuation of High-Order Harmonic Balance Solutions for Nonlinear Aeroelastic Systems," *Journal of Aircraft*, Vol. 45, No. 2, 2008, pp. 523–537. doi:10.2514/1.30472

[16] Woodgate, M. A., and Badcock, K. J., "Implicit Harmonic Balance Solver for Transonic Flow with Forced Motions," *AIAA Journal*, Vol. 47, No. 4, 2009, pp. 893–901. doi:10.2514/1.36311

[17] Campobasso, M. S., and Baba-Ahmadi, M. H., "Analysis of Unsteady Flows Past Horizontal Axis Wind Turbine Airfoils Based on Harmonic Balance Compressible Navier–Stokes Equations With Low-Speed Preconditioning," *Journal of Turbomachinery*, Vol. 134, No. 6, 2012, Paper 061020. doi:10.1115/1.4006293

[18] Ekici, K., and Hall, K. C., "Nonlinear Analysis of Unsteady Flows in Multistage Turbomachines Using the Harmonique Balance Technique," *AIAA Journal*, Vol. 45, No. 5, 2007, pp. 1047–1057. doi:10.2514/1.22888

[19] Ekici, K., and Hall, K. C., "Nonlinear Frequency-Domain Analysis of Unsteady Flows in Turbomachinery with Multiple Excitation Frequencies," *AIAA Journal*, Vol. 46, No. 8, 2008, pp. 1912–1920. doi:10.2514/1.26006

[20] Bakhle, M., Thomas, J., and Reddy, T. S. R., "Fan Flutter Computations Using the Harmonic Balance Method," *44th AIAA/ASME/SAE/ASEE Joint Propulsion Conference and Exhibit*, AIAA Paper 2008-4743, July 2008.

[21] Reddy, T. S. R., and Bakhle, M., "Aeroelastic Computations of a Compressor Stage Using the Harmonic Balance Method," *45th AIAA/ASME/SAE/ASEE Joint Propulsion Conference and Exhibit*, AIAA Paper 2009-5420, Aug. 2009.

[22] Ekici, K., and Hall, K. C., "Harmonic Balance Analysis of Limit Cycle Oscillations in Turbomachinery," *AIAA Journal*, Vol. 49, No. 7, 2011, pp. 1478–1487. doi:10.2514/1.J050858

[23] May, M., Mauffrey, Y., and Sicot, F., "Numerical Flutter Analysis of Turbomachinery Bladings Based on Time-Linearized, Time-Spectral and Time-Accurate Simulations," *15th International Forum on*

Aeroelasticity and Structural Dynamics, International Forum on Aeroelasticity and Structural Dynamics Paper IFASD-2011-080, June 2011.

[24] Erdos, J. I., Alznert, E., and McNally, W., "Numerical Solution of Periodic Transonic Flow Through a Fan Stage," *AIAA Journal*, Vol. 15, No. 11, 1977, pp. 1559–1568. doi:10.2514/3.60823

[25] Van Zante, D., Chen, J., Hathaway, M., and Chriss, R., "The Influence of Compressor Blade Row Interaction Modeling on Performance Estimates From Time-Accurate, Multistage, Navier–Stokes Simulations," *Journal of Turbomachinery*, Vol. 130, No. 1, 2008, p. 011009. doi:10.1115/1.2775486

[26] Sicot, F., Dufour, G., and Gourdain, N., "A Time-Domain Harmonic Balance Method for Rotor/Stator Interactions," *Journal of Turbomachinery*, Vol. 134, No. 1, 2012, p. 011001. doi:10.1115/1.4003210

[27] Ekici, K., Hall, K. C., and Kielb, R. E., "Harmonic Balance Analysis of Blade Row Interactions in a Transonic Compressor," *Journal of Propulsion and Power*, Vol. 26, No. 2, 2010, pp. 335–343. doi:10.2514/1.43879

[28] Fransson, T. H., Jöcker, M., Bölcs, A., and Ott, P., "Viscous and Inviscid Linear/Nonlinear Calculations Versus Quasi 3D Experimental Cascade Data for a New Aeroelastic Turbine Standard Configuration," *Journal of Turbomachinery*, Vol. 121, No. 1, Oct. 1999, pp. 717–725.

[29] Huang, H., and Ekici, K., "An Efficient Harmonic Balance Method for Unsteady Flows in Cascades," *Aerospace Science and Technology*, Vol. 29, No. 1, 2013, pp. 144–154. doi:10.1016/j.ast.2013.02.004

[30] Lane, F., "System Mode Shapes in the Flutter of Compressor Blade Rows," *Journal of the Aeronautical Sciences*, Vol. 23, No. 1, Jan. 1956, pp. 54–66.

[31] Cinnella, P., De Palma, P., Pascazio, G., and Napolitano, M., "A Numerical Method for Turbomachinery Aeroelasticity," *Journal of Turbomachinery*, Vol. 126, No. 2, 2004, pp. 310–316. doi:10.1115/1.1738122

[32] Jameson, A., "Solution of the Euler Equations For Two Dimensional Transonic Flow by a Multigrid Method," *Applied Mathematics and Computation*, Vol. 13, Nos. 3–4, 1983, pp. 327–355. doi:10.1016/0096-3003(83)90019-X

[33] He, L., "An Euler Solution for Unsteady Flows Around Oscillating Blades," *Journal of Turbomachinery*, Vol. 112, No. 4, 1990, pp. 714–722. doi:10.1115/1.2927714

[34] McMullen, M., Jameson, A., and Alonso, J., "Acceleration of Convergence to a Periodic Steady State in Turbomachinery Flows," *39th Aerospace Sciences Meeting and Exhibit*, AIAA Paper 2001-0152, Jan. 2001.

[35] Davis, S. S., "NACA 64A010 (NASA Ames Model) Oscillatory Pitching," AGARD, TR-702, Data Set 2, 1982.

[36] Sbardella, L., and Imregun, M., "Linearized Unsteady Viscous Turbomachinery Flows Using Hybrid Grids," *Journal of Turbomachinery*, Vol. 123, No. 3, 2001, pp. 568–582. doi:10.1115/1.1371777

[37] Duta, M. C., Giles, M. B., and Campobasso, M. S., "The Harmonic Adjoint Approach to Unsteady Turbomachinery Design," *International Journal for Numerical Methods in Fluids*, Vol. 40, Nos. 3–4, 2002, pp. 323–332. doi:10.1002/(ISSN)1097-0363

[38] Campobasso, M. S., and Giles, M. B., "Effects of Flow Instabilities on the Linear Analysis of Turbomachinery Aeroelasticity," *Journal of Propulsion and Power*, Vol. 19, No. 2, 2003, pp. 250–259. doi:10.2514/2.6106

[39] McBean, I., Hourigan, K., Thompson, M., and Liu, F., "Prediction of Flutter of Turbine Blades in a Transonic Annular Cascade," *Journal of Fluids Engineering*, Vol. 127, No. 6, 2005, pp. 1053–1058. doi:10.1115/1.2060731

[40] Spalart, P. R., and Allmaras, S. R., "A One-Equation Turbulence Transport Model for Aerodynamic Flows," *30th AIAA Aerospace Sciences Meeting and Exhibit*, AIAA Paper 1992-0439, Jan. 1992.

[41] Roe, P. L., "Approximate Riemann Solvers, Parameter Vectors and Difference Schemes," *Journal of Computational Physics*, Vol. 43, No. 2, 1981, pp. 357–372. doi:10.1016/0021-9991(81)90128-5

[42] Vogt, D., and Fransson, T. H., "Turbomachinery Aeroelasticity Analyses—Everyday Business or Exceptional Challenge?," *9th European Turbomachinery Conference*, March 2011.

[43] Jameson, A., Schmidt, W., and Turkel, E., "Numerical Solutions of the Euler Equations by Finite Volume Methods Using Runge-Kutta Time-Stepping Schemes," *AIAA 14th Fluid and Plasma Dynamic Conference*, AIAA Paper 1981-1259, June 1981.

B. Epureanu
Associate Editor